RSC Advances

ROYAL SOCIETY OF CHEMISTRY

PAPER

View Article Online
View Journal | View Issue

Cite this: *RSC Adv.*, 2021, **11**, 1182

A piezoelectric poly(vinylidene fluoride) tube featuring highly-sensitive and isotropic piezoelectric output for compression†

Jiajun Guo, Min Nie * and Qi Wang

Piezoelectric polymers have aroused tremendous attention in self-powered flexible wearable electronics. However, conventional plate-like piezoelectric devices demonstrated insufficient output power and monotonous piezoelectric energy harvesting performance only in one direction, failing to accommodate the complex multi-dimensional stress field. In this study, a poly(vinylidene fluoride) tube featuring all-directional piezoelectric energy harvesting performance with excellent rebound resilience was prepared *via* a fast industrial extrusion. Benefitting from the isotropic hollow tubular structure, the piezoelectric tube experienced large deformation at a small external load and thus exhibited a strong load-amplifying function to generate the optimized output power at multi-stresses from any direction, with sensitive piezoelectric performance, quick response and mechanical robustness. Finally, the practical potential as a robust energy harvester was evaluated by harvesting small energy from irregular human motions. This study provides a facile structure designing strategy for the preparation of functional piezoelectric devices for multi-directional mechanical energy harvesting applications.

Received 26th October 2020
Accepted 30th November 2020

DOI: 10.1039/d0ra09131f

rsc.li/rsc-advances

1. Introduction

Wearable electronics, including electronic watches, smart sneakers, and electronic glasses, offer great convenience and good experience to our lives for their predominance in portability and in-time feedback of human health information such as steps, state of motions, heart rates and some other functions of human bodies.[1–4] However, the power source is still from traditional batteries, the utilization of which is inevitably restricted by limited capacity, inconvenient recharging and intractable problems of recycling.[5,6] In order to solve the issues, piezoelectric energy harvesting devices are proposed to integrate with wearable electronics to achieve the self-powering by converting wasted mechanical energy from human motions into electrical power.[7–9] The application of self-powered devices in wearable electronics was put forward by Wang in 2006,[10] where the conception of nanogenerators was first realized *via* the nanoarray-structural design of zinc oxide. The current piezoelectric energy harvesting devices are made from inorganic piezoelectric materials such as PZT,[11] $BaTiO_3$,[12] and $ZnSnO_3$.[13] The brittle nature makes them hardly biocompatible to irregular motions of human bodies, including bending and twisting, leading to structural failure and deteriorated piezoelectric performance.[14] On the other hand, piezoelectric polymers are characterized by flexibility, mechanical robustness and ease of processing, and thus are considered as promising alternatives in flexible wearable self-powered devices,[8,15,16] but a large load is often required to achieve a high power output due to the low piezoelectric constants relative to inorganic ceramics.[17,18] Therefore, the reconciliation balance between highly-efficient electromechanical conversion and mechanical durability still remains to be unsolved.

The piezoelectric performance of a given material is not only determined by the intrinsic piezoelectric attributes of polymer materials but also depends on the level of the imposed stress, which is, in turn, governed by the geometry of the corresponding device.[10,19,20] Compared to the traditional piezoelectric film with flat-surface, some unique geometries, such as porous,[21] array[22] and pyramid-shaped structures,[23] exhibited strong strain-amplifying function to maximize mechanical deformation, generating optimized output power. In fact, the first piezoelectric device composed of ZnO nanoarrays was a typical case of piezoelectric output enhancement *via* the structured design of the lever principle. However, the construction of special structures often involved complex processing techniques such as template growing,[24] chemical vapor deposition,[25] or photolithography,[26] with low efficient production.

Recently, Jung *et al.* demonstrated that curved geometry can intensify the applied stress on a piezoelectric device to enable a higher voltage output than the flat-type one.[27] When external force was acted on the curved surface, large deformation could

State Key Laboratory of Polymer Materials Engineering, Polymer Research Institute of Sichuan University, Chengdu 610065, China. E-mail: poly.nie@gmail.com; Fax: +86-28-85402465; Tel: +86-28-85405133

† Electronic supplementary information (ESI) available. See DOI: 10.1039/d0ra09131f

be generated at the direction of imposed force due to the concentrated stress. Yang *et al.* successfully utilized the curved structure to obtain increased piezoelectric output from ~1 V to ~2 V.[28] Though effective in stress amplification and piezoelectric enhancement, the preparation of a curved structure is a multi-step process with low efficiency: first, the piezoelectric film was prepared and then prestrained to maintain the curved structure.[20,29,30] More importantly, this curved structure can gradually return to the plain structure at increased loading cycles and only works at vertical loading perpendicular to the curved surface, unable to accommodate the complex stress field from all directions in practice applications.

It is well-known that a tubular structure is naturally curved in any direction and can be formed directly *via* industrial continuous extrusion featuring highly-efficient production. Accordingly, the piezoelectric tube is expected to exhibit promising potential in piezoelectric conversion. Herein, we chose poly(-vinylidene fluoride-*co*-hexafluoropropene) (P(VDF–HFP)) as a model polymer because the presence of hexafluoropropylene exerted a large steric hindrance to the PVDF chain to facilitate the formation of all-trans conformation and obtain electroactive β-crystals in normal melt-processing. Then, the conventional extrusion of the polymer tube was adopted to prepare a tubular piezoelectric device. The piezoelectric performance of tubular devices and working mechanisms were systematically investigated based on experiment and finite element simulation analysis. Compared to traditional plate-like structures, the tubular device possessed a smaller load threshold of piezoelectric output and was successfully utilized for harvesting energy from different human motions. This study provides a structure designing strategy for the preparation of highly-efficient piezoelectric devices.

2. Experiment section

2.1. Materials

PVDF–HFP was purchased from Sigma-Aldrich Co., Ltd. The weight-average molecular weight was ~400 000 g mol^{-1}, with a piezoelectric coefficient of ~20 pC N^{-1}.[31]

2.2. Sample preparation

PVDF–HFP pellets were fed into a conventional tube extruder with a screw and die with temperatures of 220 °C and 230 °C, respectively, obtaining the tube with an outer diameter of 4.36 mm and a wall thickness of 0.27 mm. The length of the tube was controlled to 10 mm for the following testing.

As a control, PVDF–HFP pellets were thermal-compressed into a plate-like sample with a thickness of 0.27 mm at 230 °C. Then, the size was cut to an area ~140 mm^2, comparable to the value of the 10 mm-long tube.

2.3. Characterization

Measurement of piezoelectric performance. To evaluate the piezoelectric performance and energy harvesting prospect, the output voltage signals were recorded by a Keithley-6514 system electrometer. The impact force was exerted by a BOSE 3220 SERIES II universal testing machine (BOSE, Co., USA). The measured frequency was 1 Hz. The corresponding displacement–stress curves and output voltages were recorded.

In addition, the charging measurement circuit was developed by integrating a tubular piezoelectric device, a rectifier, a 1 μF capacitor and CHI660E 413054 electrochemical workstation (Shanghai Chen Hua Co., Ltd, China). The charging energy was recorded by the electrochemical workstation.

Simulation of vertical compression. To provide detailed research on mechanical behaviors, the finite element analysis was conducted using the Abaqus CAE 6.14 software. The Young's modulus and Poisson's ratio used for simulation were 900 MPa and 0.4, respectively. The sample model was placed between a rigid body and a fixed rigid plain. Vertical loading was exerted on the rigid body. The resultant visualization of stress distribution was then recorded.

3. Results and discussions

3.1. Stress and piezoelectric behaviors at different compressing loads

It is well known that the piezoelectric output highly relies on the applied stress as determined by structural features. The piezoelectric loading threshold triggering piezoelectric output generation reflects the sensitivity of a piezoelectric device to an external load and is a key factor for determining the successful application for harvesting low-frequency mechanical energy from the daily human motion. In order to verify the amplification effect of the tubular structure on the piezoelectric output, a compression load was imposed on the plate- (FS) and tube-like (TS) samples, and the corresponding compression displacement with stress and piezoelectric signals were recorded synchronously, as shown in Fig. 1. Although the two samples had similar instantaneous remnant polarization (the corresponding information is available in the ESI, Fig. S1†), the different piezoelectric properties were investigated. For the plate-like sample, no distinct piezoelectric signals appeared at an external load less than 1 N, except for some noise from static electricity in the air;[32] the load threshold was 1.25 N, where the mutational piezoelectric signal with an open-circuit voltage of ~0.3 V, was generated. On the contrary, the tubular sample exhibited a lower load threshold of 0.3 N, with a high piezoelectric output of ~0.4 V. One can notice that the two samples had similar compression displacement at the critical loads: 0.45% for the plate-like sample and 0.52% for the tubular sample. This sufficiently demonstrated the stress amplification effect of the tubular structure, allowing for large deformation generated at a smaller load. This amplification mechanism should be analogous to the reported curved structure.[33]

Further, the finite element analysis (FEA) was carried out to reveal the structural dependence of mechanical deformation. Under a compression load, the plate-like sample experienced homogeneous deformation with part stress concentration at the edge and the stress concentrated 8–9 kPa at the load threshold of 1.25 N, which was consistent with the average value of 9 kPa calculated based on the simple stress equation, $\sigma = F/S$ (the corresponding information is available in the ESI, Fig. S2†). On

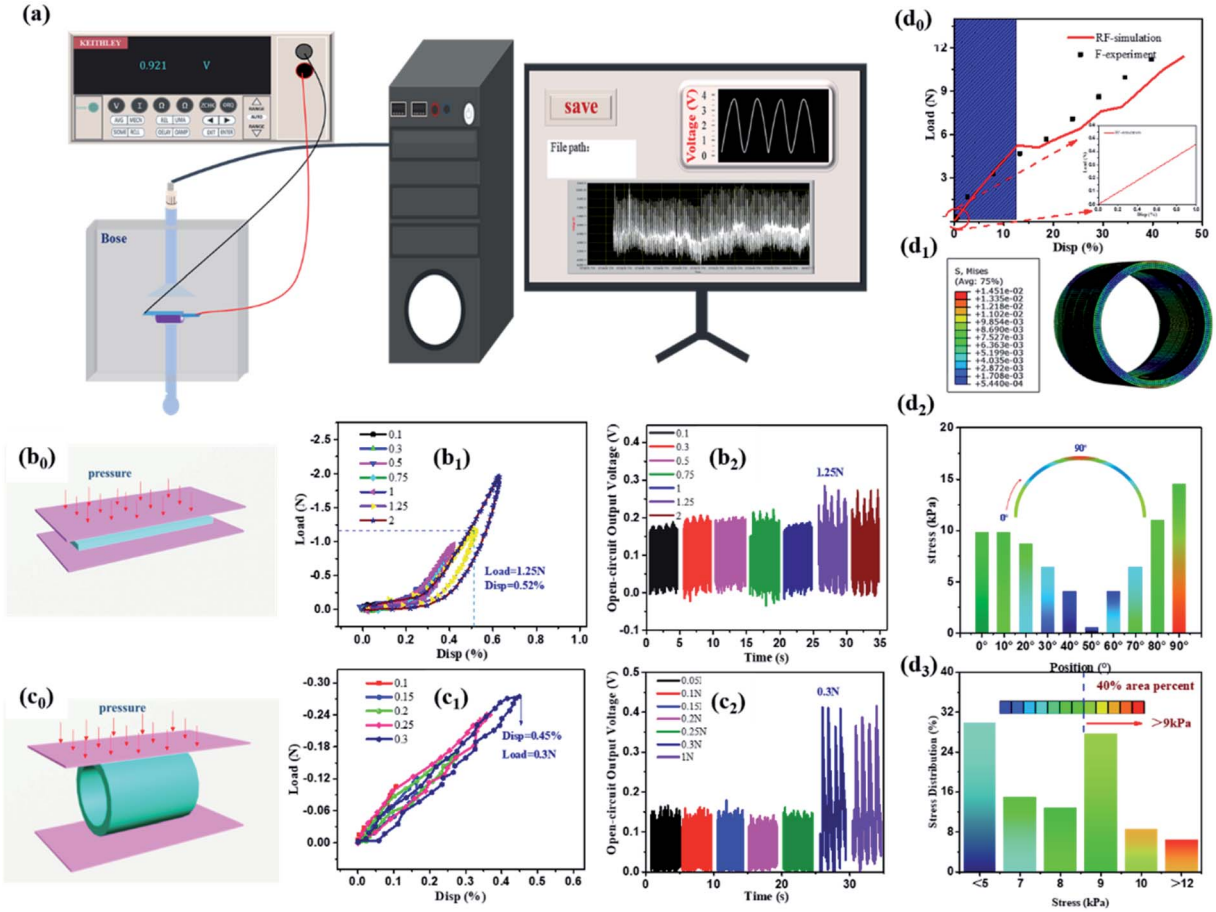

Fig. 1 Study on the critical loading threshold of piezoelectric signals: schematic of the piezoelectric output test (a); vertical compression model of FS (b_0) and TS (c_0); the stress–strain curves of FS (b_1) and TS (c_1) under different lateral compression loads; the corresponding piezoelectric performance of FS (b_2) and TS (c_2); load–displacement curves (d_0) of PVDF tube, wherein dark dots from the experimental data were consistent with the simulated value (red line); two-dimensional stress distribution pattern (d_1), the stress as a function of angle in a quarter area (d_2) and statistical results of stress distribution (d_3) at the corresponding load threshold of 0.3 N.

the contrary, the tubular sample exhibited different stress characteristics. It can be seen from Fig. $1d_0$ that with the increase in the external load, the PVDF tube experienced elastic and plastic deformation. As the plastic deformation affected the dimensional stability and the final application, the experimental results deviated from the simulation. However, the load–displacement relationship during the elastic deformation stage of 12% displacement fitted well with the simulated result, verifying the validity of FEA. When a compression load was imposed on the tubular sample, asymmetric stress distribution was generated along the hoop direction: maximum stress appeared at the top and bottom sides, followed by a lower value at the left and right sides with minimum deformation at ±45° and ±225° off the meridian, as reflected by the stress distribution in a quarter area as presented in Fig. $1d_1$ and 2. The statistical results of stress distribution at the load threshold of 0.3 N indicated that ~40% area of the tubular sample was subjected to a higher stress of ≥9 kPa, which was critical stress initiating piezoelectric output, as shown in Fig. $1d_3$. This amplification of local deformation should be responsible for the enhanced piezoelectric sensitivity at a small external load, beneficial for harvesting mechanical energy from human motions.

3.2. Piezoelectric features of tubular devices

Compared to a single working mode of the conventional curved piezoelectric device limited under vertical load, a PVDF tube can equally accommodate multi-stresses from any direction in practice application due to the isotropic nature of the tubular structure. As presented in Fig. 2a, the stress value and distributions were the same under different loads along with the vertical, oblique and lateral directions. The adaptability of multi-directional stress ensured the PVDF tube to effectively harvest energy in a complex stress field, as referred to by the same piezoelectric signals in all directions. Moreover, one can notice that the tubular harvesting device presented a rapid response towards external force with stable output due to well rebound resilience. Inset in Fig. 2b showed the piezoelectric output after one cycle. The response time to the piezoelectric signal was calculated to be ~81 ms based on the time span from 10% to 90% of the piezoelectric peak, which was comparable to

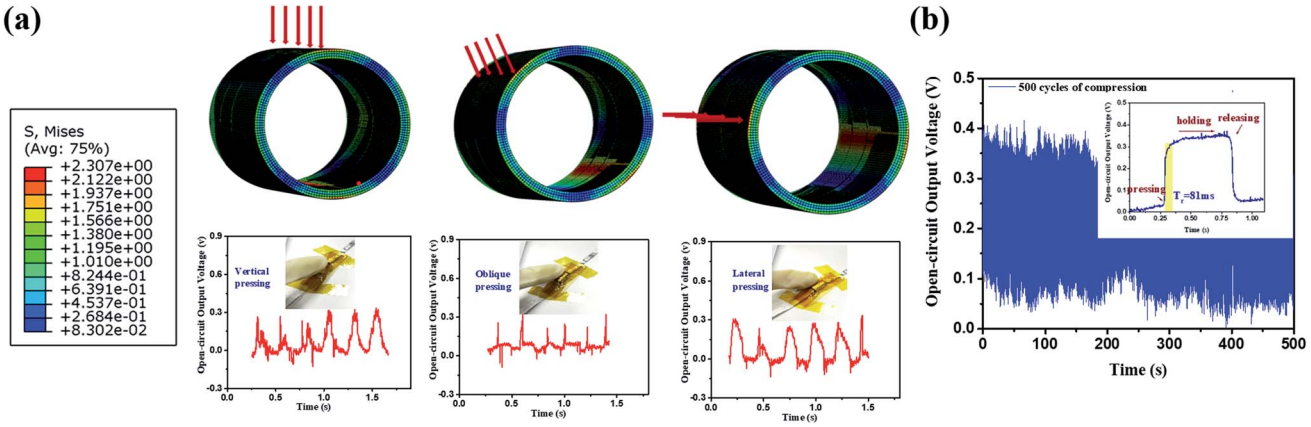

Fig. 2 Studies on piezoelectric features of TS: visualization of stress at the vertical, oblique and lateral direction with a piezoelectric output at the corresponding compression direction (a); the piezoelectric performance after 500 cycles with the inset of the piezoelectric output after one cycle (b).

the value obtained from reported sensitive piezoelectric structures.[28,34] Due to the rapid response towards external force at small loading, the PVDF tube was mechanically robust and could sustain stable output performance for over 500 cycles of repeated mechanical deformation, suggesting the potential for a long-term application. Accordingly, it can be concluded safely that benefitting from the unique hollow tubular structure the PVDF tube is characterized by a sensitive piezoelectric performance at low load, quick response at any direction, mechanical robustness, providing the possibility of robust energy harvesting application from complex stress occasion.

3.3 Energy harvesting applications

Finally, the practical potential of the PVDF tube as a robust energy harvester was evaluated by harvesting small energy from irregular motions of different body regions. Accordingly, the PVDF tube was attached to different parts of human bodies, as shown in Fig. 3a. It can be noticed from Fig. 3b–d that the distinct piezoelectric outputs were generated by tensile and compression loads from wrist bending, finger bending and walking, successfully verifying that the as-prepared PVDF tube indeed adapted to various loads and generated effective piezoelectric outputs. In addition, a capacitor of 1 μF was used as an energy storage system and the charging energy was studied by deforming the piezoelectric tube (Fig. 3e). By periodically bending of finger or wrist and walking, the capacitor was charged to ~1.2 V by wrist bending, 0.7 V by finger bending or walking for 100 s. These charging characteristics demonstrated that tubular devices possessed a promising prospect for energy harvesting in wearable devices and energy harvesting at complex external load.

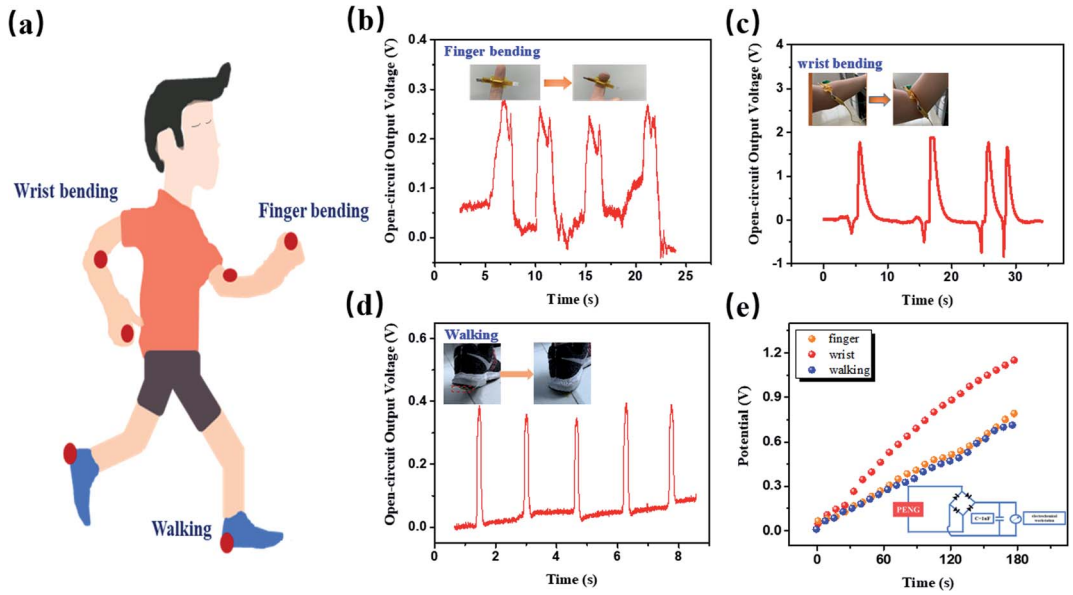

Fig. 3 Piezoelectric energy harvesting application of TS on the human body: potential mechanical source generated by movement (a); piezoelectric performance at finger bending (b), wrist joint bending (c), walking (d) and their charging curves (e).

4. Conclusions

In this study, the isotropic tubular structure of PVDF–HFP was designed for energy harvesting at a multi-dimensional stress field *via* melt extrusion. The FEM and experimental results showed that the tubular structure exhibited the load-amplifying function, leading to a smaller piezoelectric loading threshold of 0.3 N, which was far lower than 1.25 N for the plate-like sample. This stress amplification effect and isotropic nature of the tubular structure ensured the equal accommodation for multi-stresses from any direction with a quick response and mechanical robustness. Finally, the as-prepared piezoelectric tube was successfully applied to harvest small energy from irregular human motions, demonstrating that the tubular structure is a promising candidate for preparing a high-performance piezoelectric device.

Conflicts of interest

There are no conflicts to declare.

Acknowledgements

This work is financiered by the National Natural Science Foundation of China (51933007, 51873130, 51721091 and 51703182).

References

1 W. Zhang, C. Hou, Y. Li, Q. Zhang and H. Wang, *Nanoscale*, 2017, **9**, 17821–17828.
2 Y. Khan, A. E. Ostfeld, C. M. Lochner, A. Pierre and A. C. Arias, *Adv. Mater.*, 2016, **28**, 4373–4395.
3 C. Yan, W. Deng, L. Jin, T. Yang, Z. Wang, X. Chu, H. Su, J. Chen and W. Yang, *ACS Appl. Mater. Interfaces*, 2018, **10**, 41070–41075.
4 S. Y. Chung, H.-J. Lee, T. I. Lee and Y. S. Kim, *RSC Adv.*, 2017, **7**, 2520–2526.
5 Q. Wang, P. Ping, X. Zhao, G. Chu, J. Sun and C. Chen, *J. Power Sources*, 2012, **208**, 210–224.
6 C. Y. Jhu, Y. W. Wang, C. M. Shu, J. C. Chang and H. C. Wu, *J. Hazard. Mater.*, 2011, **192**, 99–107.
7 M. A. Barique, Y. Neo, M. Noyori, L. Aprila, M. Asai and H. Mimura, *Nanotechnol*, 2020, **32**, 015401.
8 M. Zhu, S. S. Chng, W. Cai, C. Liu and Z. Du, *RSC Adv.*, 2020, **10**, 21887–21894.
9 C. Lu, L. Zhang, C. Xu, Z. Yin, S. Zhou, J. Wang, R. Huang, X. Zhou, C. Zhang, W. Yang and J. Lu, *RSC Adv.*, 2016, **6**, 67400–67408.
10 Z. L. Wang and J. H. Song, *Science*, 2006, **312**, 242–246.
11 K. Zhang, S. Wang and Y. Yang, *Adv. Energy Mater.*, 2016, **7**, 1601852.
12 Y. Kim, K. Y. Lee, S. K. Hwang, C. Park, S.-W. Kim and J. Cho, *Adv. Funct. Mater.*, 2014, **24**, 6262–6269.
13 S. Paria, S. Ojha, S. K. Karan, S. K. Si, R. Bera, A. K. Das, A. Maitra, L. Halder, A. De and B. B. Khatua, *ACS Appl. Electron. Mater.*, 2020, **2**, 2565–2578.
14 E. L. Tsege, G. H. Kim, V. Annapureddy, B. Kim, H.-K. Kim and Y.-H. Hwang, *RSC Adv.*, 2016, **6**, 81426–81435.
15 F. R. Fan, W. Tang and Z. L. Wang, *Adv. Mater.*, 2016, **28**, 4283–4305.
16 H. B. Kang, C. S. Han, J. C. Pyun, W. H. Ryu, C.-Y. Kang and Y. S. Cho, *Compos. Sci. Technol.*, 2015, **111**, 1–8.
17 X. Hu, S. Yu and B. Chu, *Mater. Des.*, 2020, **192**, 108700.
18 S. Ahn, Y. Cho, S. Park, J. Kim, J. Sun, D. Ahn, M. Lee, D. Kim, T. Kim, H. Shin and J.-J. Park, *Nano Energy*, 2020, **74**, 104932.
19 N. A. Shepelin, A. M. Glushenkov, V. C. Lussini, P. J. Fox, G. W. Dicinoski, J. G. Shapter and A. V. Ellis, *Energy Environ. Sci.*, 2019, **12**, 1143–1176.
20 Y.-H. Shin, I. Jung, M.-S. Noh, J. H. Kim, J.-Y. Choi, S. Kim and C.-Y. Kang, *Appl. Energy*, 2018, **216**, 741–750.
21 W. Tong, Q. An, Z. Wang, Y. Li, Q. Tong, H. Li, Y. Zhang and Y. Zhang, *Adv. Mater.*, 2020, e2003087, DOI: 10.1002/adma.202003087.
22 J. Wang, J. Jiang, C. Zhang, M. Sun, S. Han, R. Zhang, N. Liang, D. Sun and H. Liu, *Nano Energy*, 2020, **76**, 105050.
23 J.-H. Lee, H.-J. Yoon, T. Y. Kim and M. K. Gupta, *Adv. Funct. Mater.*, 2015, **25**, 3203–3209.
24 A. Datta, Y. S. Choi, E. Chalmers, C. Ou and S. Kar-Narayan, *Adv. Funct. Mater.*, 2017, **27**, 1604262.
25 T. Lim, G. Ico, K. Jung, K. N. Bozhilov, J. Nam and A. A. Martinez-Morales, *CrystEngComm*, 2018, **20**, 5688–5694.
26 G. Tian, D. Xiong, Y. Su, T. Yang, Y. Gao, C. Yan, W. Deng, L. Jin, H. Zhang, X. Fan, C. Wang, W. Deng and W. Yang, *Nano Lett.*, 2020, **20**, 4270–4277.
27 W.-S. Jung, M.-J. Lee, M.-G. Kang, H. G. Moon, S.-J. Yoon, S.-H. Baek and C.-Y. Kang, *Nano Energy*, 2015, **13**, 174–181.
28 T. Yang, H. Pan, G. Tian, B. Zhang, D. Xiong, Y. Gao, C. Yan, X. Chu, N. Chen, S. Zhong, L. Zhang, W. Deng and W. Yang, *Nano Energy*, 2020, **72**, 104706.
29 I. Jung, Y.-H. Shin, S. Kim, J.-y. Choi and C.-Y. Kang, *Appl. Energy*, 2017, **197**, 222–229.
30 S. Wang, C. Wang, Z. Gao and H. Cao, *Appl. Energy*, 2020, **276**, 115512.
31 Y. Wu, J. Qu, W. A. Daoud, L. Wang and T. Qi, *J. Mater. Chem. A*, 2019, **7**, 13347–13355.
32 S. K. Karan, S. Maiti, A. K. Agrawal, A. K. Das, A. Maitra, S. Paria, A. Bera, R. Bera, L. Halder, A. K. Mishra, J. K. Kim and B. B. Khatua, *Nano Energy*, 2019, **59**, 169–183.
33 Y. Li, K. Zhang, M. Nie and Q. Wang, *Ind. Eng. Chem. Res.*, 2019, **58**, 22273–22282.
34 J. Yan, Y. Han, S. Xia, X. Wang, Y. Zhang, J. Yu and B. Ding, *Adv. Funct. Mater.*, 2019, **29**, 1907919.